Chirurgia (Bucur). 2026 July, Online Ahead of Print

http://dx.doi.org/10.21614/chirurgia.3336

# Morphological Variability of the P1 Segment of the Posterior Cerebral Artery: An Anatomical and Angiographic Study with Clinical Correlations

**Ionuț Bulbuc, Constantin Dina*, Constantin Ionescu, Andrei Rusali, Bogdan Marian Caraban**

Faculty of Medicine, Ovidius University of Constanța, Constanța, Romania

***Corresponding author:**
Constantin Dina, MD
Faculty of Medicine
Ovidius University of Constanța
Constanța, Romania
E-mail: constantin.dina@gmail.com

Received: 30.04.2026
Accepted: 18.06.2026

## Rezumat

***Variabilitatea morfologică a segmentului P1 al arterei cerebrale posterioare: particularități anatomo-angiografice și considerații clinice***

*Scop:* Segmentul precomunicant (P1) al arterei cerebrale posterioare (ACP) este un segment arterial scurt, dar important din punct de vedere clinic, al cărui calibru, lungime şi distribuție a ramurilor perforante influențează hemodinamica circulației posterioare, ischemia talamo-mezencefalică şi managementul anevrismelor arterei comunicante posterioare (AComP). Scopul acestui studiu a fost caracterizarea morfologiei segmentului P1 pe baza unei serii combinate de date anatomice şi imagistice şi discutarea rezultatelor în raport cu implicațiile clinice ale acestora pentru interpretarea radiologică şi procedurile neurovasculare.

*Metode:* Au fost evaluate în total 320 de cazuri: 20 de specimene cerebrale fixate în formol (10 injectate cu material plastic), 120 de angiografii CT (CTA) şi 180 de angiografii RMN (MRA). Au fost înregistrate lungimea segmentului P1, calibrul P1, simetria dreapta–stânga, hipoplazia, agenezia, fenestrația, configurația de tip fetal a ACP, modelul ramurilor perforante posteromediale şi originea arterei cerebeloase superioare (ACS). Măsurătorile au fost revizuite independent de doi radiologi seniori, cu rezolvarea neconcordanțelor prin consens. Măsurătorile morfometrice cantitative au fost efectuate numai pe seturile de date angiografice. Comparațiile morfometrice între partea dreaptă şi cea stângă au fost efectuate utilizând testul U Mann-Whitney pentru eşantioane independente, deoarece identificatorii cazurilor individuale nu au fost disponibili pentru a permite o analiză pereche.

*Rezultate:* Lungimea medie a segmentului P1 a fost de 7,57 ± 2,24 mm pe partea dreaptă (n = 255) şi de 7,38 ± 2,19 mm pe partea stângă (n = 254). Calibrul mediu al P1, incluzând segmentele hipoplazice, a fost de 1,87 ± 0,59 mm pe partea dreaptă şi de 1,86 ± 0,57 mm pe partea stângă. Hipoplazia P1, definită printr-un calibru < 1 mm, a fost observată în 51 de cazuri (15,9%), agenezia P1 în 6 cazuri (1,9%), iar fenestrația P1 în 3 cazuri (0,9%). Au fost identificate cinci modele ale ramurilor perforante posteromediale, tipurile asimetrice reprezentând 59,4% dintre cazuri, iar modelul de arteră Percheron fiind prezent în 5 cazuri (1,6%). ACS a avut origine din P1 în 25 de cazuri (7,8%), incluzând 3 origini contralaterale.

*Concluzie:* Lungimea P1 şi calibrul mediu au fost în mare măsură simetrice între cele două părți, însă variantele relevante clinic, adică hipoplazia, agenezia, fenestrația, ACP de tip fetal, modelele asimetrice ale ramurilor perforante, artera Percheron şi

originea ACS din P1, au fost suficient de frecvente pentru a susține raportarea sistematică a complexului P1–AComP la examinările CTA şi MRA.

**Cuvinte cheie:** arteră cerebrală posterioară, segment P1, arteră cerebrală posterioară de tip fetal, artera Percheron, angiografie CT, angiografie RMN

## Abstract

*Purpose:* The precommunicating (P1) segment of the posterior cerebral artery (PCA) is a short but clinically important arterial segment whose calibre, length and perforator distribution influence posterior circulation haemodynamics, thalamo-mesencephalic ischaemia and the management of posterior communicating artery (PComA) aneurysms. The aim of this study was to characterize the morphology of the P1 segment in a combined anatomical and angiographic series and to discuss the findings in relation to their clinical implications for radiological interpretation and neurovascular procedures.
*Methods:* A total of 320 cases were evaluated: 20 formalin-fixed brain specimens (10 plastic-injected), 120 CT angiographies (CTA) and 180 MR angiographies (MRA). P1 length, P1 calibre, right–left symmetry, hypoplasia, agenesis, fenestration, fetal-type PCA configuration, posteromedial perforator pattern and superior cerebellar artery (SCA) origin were recorded. Quantitative morphometric measurements were performed only on the angiographic datasets. Measurements were reviewed independently by two senior radiologists with consensus adjudication. Right–left morphometric comparisons were performed with the Mann–Whitney U test on independent samples, because individual case identifiers were not available to support paired analysis.
*Results:* Mean P1 length was 7.57 ± 2.24 mm on the right (n = 255) and 7.38 ± 2.19 mm on the left (n = 254). Mean P1 calibre including hypoplastic segments was 1.87 ± 0.59 mm on the right and 1.86 ± 0.57 mm on the left. P1 hypoplasia (calibre < 1 mm) was observed in 51 cases (15.9 %), P1 agenesis in 6 (1.9 %) and P1 fenestration in 3 (0.9 %). Five posteromedial perforator patterns were described using an exploratory framework proposed in this study, with asymmetric patterns representing 59.4 % of cases and an artery of Percheron pattern in 5 cases (1.6 %). The SCA arose from P1 in 25 cases (7.8 %), including 3 contralateral origins.
*Conclusion:* P1 length and mean calibre were broadly symmetric between sides, but clinically relevant variants — hypoplasia, agenesis, fenestration, fetal-type PCA, asymmetric perforator patterns, artery of Percheron, and SCA origin from P1 — were frequent enough to support systematic reporting of the P1–PComA complex on CTA and MRA. The proposed perforator scheme is exploratory and requires external clinical–radiological validation.

**Keywords:** posterior cerebral artery, P1 segment, fetal-type posterior cerebral artery, artery of Percheron, CT angiography, MR angiography

## Introduction

The posterior cerebral artery (PCA) is the terminal branch of the basilar artery in the adult configuration of the posterior cerebral circulation. It supplies the occipital lobe, the posteromedial temporal region, the thalamus, the rostral midbrain, posterior choroidal territories, and several deep perforator-dependent structures (1-3). Through its connection with the posterior communicating artery (PComA), the PCA also contributes to the posterior part of the cerebral arterial circle and represents a functional interface between the vertebrobasilar and internal carotid systems (4,5).

The P1 segment, also termed the precommunicating segment, extends from the basilar bifurcation to the junction with the PComA. Although short, this segment has disproportionate clinical significance: it contributes to PCA inflow, gives rise to thalamo-mesencephalic perforators, and determines whether the PCA territory is supplied predominantly by the basilar artery or by the internal carotid artery (ICA) through the PComA (1,2,6,7).

Variations in P1 calibre and development include hypoplasia, agenesis, fenestration, and fetal-type PCA configurations. The fetal-type PCA derives embryologically from persistence of the embryonic carotid contribution to the posterior circulation, in which the

PComA remains the dominant supply to the PCA territory (8,9). This configuration is clinically relevant because emboli arising from the ICA may involve an apparently posterior territory, whereas basilar artery occlusion may spare an occipital territory supplied through a fetal-type PComA (10,11).

P1 variations also influence the distribution of deep perforating arteries. These vessels supply densely organized neural structures within the paramedian thalamus and rostral midbrain, and small perforator infarctions may therefore cause complex neurological syndromes including oculomotor palsy, hemiparesis, ataxia, sensory deficits, altered consciousness, and alternating brainstem syndromes (6,7,12,13,14).

The aim of this study was to evaluate the morphology of the P1 segment of the PCA in a combined anatomical and angiographic series and to correlate the findings with published data and clinical implications relevant to radiological interpretation, stroke topography, aneurysm haemodynamics, and neurovascular procedures. Following the established tradition of surgical anatomy studies, clinical correlation is understood here as the structured linkage of morphological variants documented in the present series with their known implications for radiological reporting and neurovascular management, based on the published literature; the study did not include direct clinical follow-up of the patients whose imaging datasets were analysed.

## Materials and Methods

### *Study Design*

This study was designed as a descriptive anatomical and angiographic investigation supplemented by a narrative review of clinically relevant literature. The original component focused on the morphology and morphometry of the P1 segment of the PCA. The clinical correlation component addressed fetal-type PCA, perforator variability, the artery of Percheron, superior cerebellar artery (SCA) origin from P1, alternating midbrain syndromes, and haemodynamic mechanisms relevant to PComA aneurysms.

### *Study Material*

The study included 320 cases. The material consisted of 20 formalin-fixed brain specimens, 120 CT angiographies (CTA), and 180 MR angiographies (MRA) (*Table 1*). Ten of the anatomical specimens were injected with plastic material to improve visualization of the arterial tree. All cases were evaluated from an anatomical perspective; associated pathology was not used as an inclusion or exclusion criterion for the descriptive anatomical analysis.

**Table 1.** Study material.

| Study component | Number of cases | Percentage (n=320) |
|---|---|---|
| Anatomical dissections | 20 | 6.3 % |
| CT angiography | 120 | 37.5 % |
| MR angiography | 180 | 56.3 % |
| Total | 320 | 100.0 % |

### *Inclusion and Exclusion Criteria*

CTA and MRA datasets were included when the basilar apex, the P1 segments, and the PComA region were sufficiently visualized for anatomical assessment. Datasets with incomplete coverage of the basilar apex, major motion artifacts, severe vascular distortion, or insufficient post-processing quality were excluded from quantitative morphometry but could be retained for qualitative anatomical discussion when the relevant variant was clearly visible. The exclusion flow leading to the per-parameter denominators reported in *Tables 2-4* is summarized in *Fig. 1* (STROBE-style flowchart).

### *Imaging Protocol and Post-Processing*

MRA examinations were performed on a GE Pioneer 1.5 T 16-channel system. The vascular protocol combined a three-dimensional time-of-flight (3D TOF) angiographic sequence for arterial visualization of the basilar apex, P1 segments and PComA, with an isotropic 3D T2-weighted CUBE acquisition for high-resolution anatomical correlation of perivascular structures. CTA examinations were performed on a GE 128-slice multidetector CT scanner; iodinated contrast agent was injected intravenously at a flow

**Table 2.** Descriptive statistics for P1 length on the angiographic dataset (CTA and MRA combined).

| Parameter | Right P1 | Left P1 |
|---|---|---|
| n | 255 | 254 |
| Mean (mm) | 7.57 | 7.38 |
| SD (mm) | 2.24 | 2.19 |
| Median (mm) | 7.40 | 7.20 |
| IQR (mm) | 6.20–8.65 | 6.00–8.60 |
| Min (mm) | 2.00 | 2.00 |
| Max (mm) | 18.40 | 17.70 |

All values reflect the angiographic luminal diameter measured on CTA and MRA datasets. Denominators differ from N = 320 because the cadaveric subset (n = 20) was not included in the morphometric analysis, and a small number of angiographic cases were excluded for measurement reliability (see *Fig. 1*).

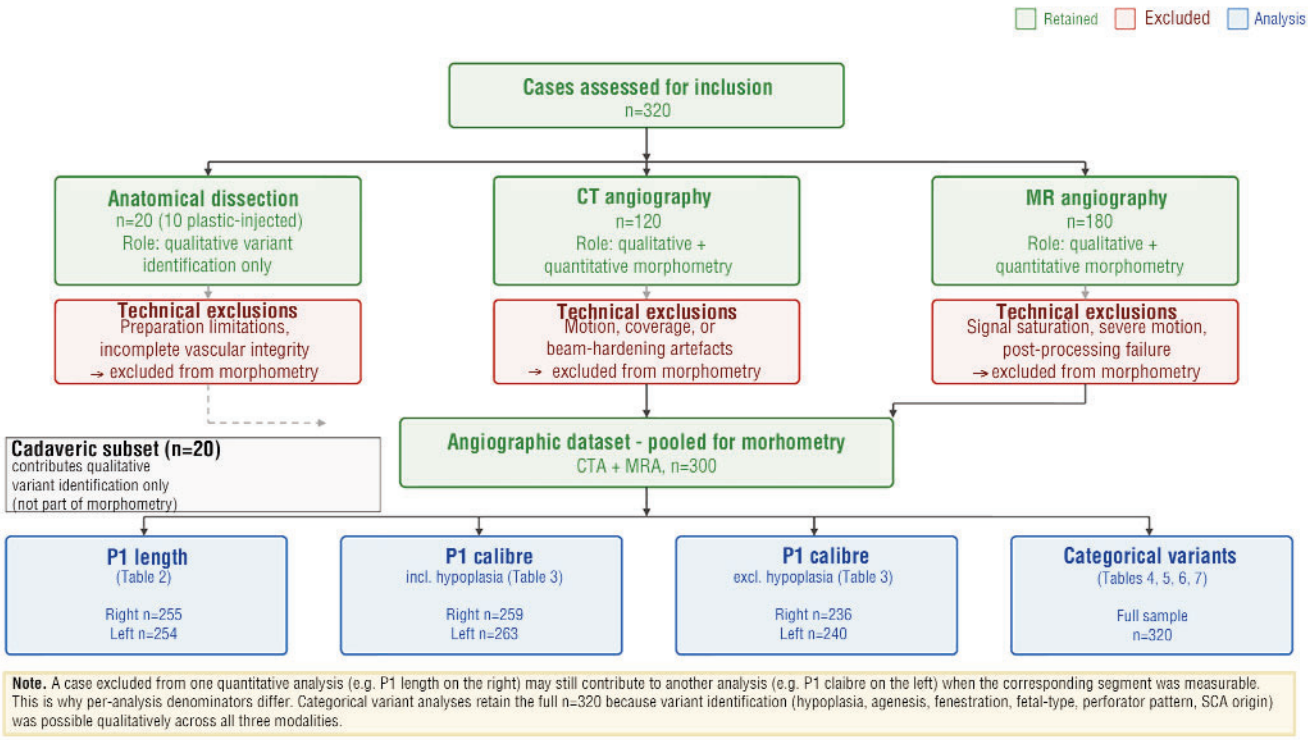


**Figure 1.** Flow diagram of case selection and per-analysis denominators (STROBE-style).
***Assessed for inclusion:*** 320 cases in total — 20 formalin-fixed brain specimens (10 plastic-injected), 120 CT angiographies (CTA) and 180 MR angiographies (MRA).
***Contribution by modality:*** The cadaveric subset (n = 20) contributed qualitative variant identification only (perforator distribution, fenestration, agenesis, SCA origin from P1) and was not included in the morphometric analysis. Morpho-metric measurements (P1 length and P1 calibre) were therefore performed only on the angiographic dataset (CTA + MRA, n = 300).
***Per-analysis exclusion reasons and evaluable denominators:*** • P1 length (*Table 2*): excluded from the angiographic dataset because of motion, coverage or beam-hardening artefacts on CTA or signal saturation, severe motion or post-processing failure on MRA. Retained: right n = 255, left n = 254. • P1 calibre including hypoplastic segments (*Table 3*): excluded because of the same technical reasons as above. Retained: right n = 259, left n = 263. • P1 calibre excluding hypoplastic segments (*Table 3*): further exclusion of hypoplastic segments (calibre < 1 mm) from the corresponding subset. Retained: right n = 236, left n = 240. • Categorical variant analyses (*Tables 4, 5, 6, 8*): hypoplasia, agenesis, fenestration, fetal-type configuration, perforator pattern, and SCA origin from P1 were assessed qualitatively across all three modalities. The full denominator n = 320 was retained, with the cadaveric subset contributing qualitative confirmation only.
**Note:** A case excluded from one quantitative analysis (e.g. P1 length on the right) could still contribute to another analysis (e.g. P1 calibre on the left) when the corresponding segment was measurable. This explains why denominators differ between morphometric variables and sides.

**Table 3.** Descriptive statistics for P1 calibre on the angiographic dataset (CTA and MRA combined), including and excluding hypoplastic segments.

| Parameter | Right — incl. hypoplasia | Left — incl. hypoplasia | Right — excl. hypoplasia | Left — excl. hypoplasia |
|---|---|---|---|---|
| n | 259 | 263 | 236 | 240 |
| Mean (mm) | 1.87 | 1.86 | 1.98 | 1.98 |
| SD (mm) | 0.59 | 0.57 | 0.48 | 0.43 |
| Median (mm) | 1.90 | 1.90 | 1.95 | 1.90 |
| IQR (mm) | 1.60–2.30 | 1.60–2.20 | 1.60–2.30 | 1.70–2.30 |
| Min (mm) | 0.30 | 0.30 | 1.00 | 1.00 |
| Max (mm) | 3.70 | 3.80 | 3.70 | 3.80 |

**Note.** The denominator differs from n = 320 because P1 calibre was measured only on the angiographic dataset (CTA + MRA); the cadaveric subset (n = 20) contributed qualitative variant confirmation only. Within the angiographic dataset, right (n = 259 / 236) and left (n = 263 / 240) denominators reflect the exclusion of hypoplastic segments in the corresponding analysis. See Fig. 1 for the full case-selection flow.

**Table 4.** Symmetry and dominance of P1 calibre

| Configuration | Number of cases | Percentage (n=320) |
|---|---|---|
| Right–left symmetry (Δ ≤ 0.3 mm) | 212 | 66.2 % |
| Right-sided dominance | 55 | 17.2 % |
| Left-sided dominance | 49 | 15.3 % |
| Borderline / unclassified | 4 | 1.3 % |
| Total | 320 | 100.0 % |

**Note.** Categorical variant analysis was performed on the full sample (n = 320) because right-versus-left dominance of P1 calibre could be classified qualitatively across all three modalities, including in cases where the exact millimetre-level measurement was not reliable.

rate of 5 mL/s, and acquisition was reconstructed at a slice thickness of 1.5 mm. All datasets were transferred to a GE Advantage Workstation 4.7, where three-dimensional volume-rendering (VRT) and maximum intensity projection (MIP) reconstructions were generated; morphometric measurements were performed on the workstation using the standard distance and diameter tools. Datasets were reviewed independently by two senior radiologists, and disagreements were resolved by consensus.

### *Anatomical Definitions and Measured Parameters*

The P1 segment was defined as the arterial segment extending from the basilar artery bifurcation to the junction with the PComA. Quantitative morphometric measurements (P1 length and P1 calibre) were performed only on the angiographic datasets (CTA and MRA), where calibrated digital tools allowed reproducible distance and diameter measurements; the cadaveric specimens were used for qualitative anatomical confirmation and for the identification of variants (perforator distribution, fenestration, agenesis, SCA origin from P1) but were not included in the morphometric series. P1 length was measured along the central axis of the vessel from the basilar bifurcation to the PComA junction, on three-dimensional angiographic reconstructions. P1 calibre was measured perpendicular to the local vessel axis on the clearest available segment; in irregular or hypoplastic segments, the minimum reproducible luminal diameter was retained for classification. All morphometric values therefore reflect the angiographic luminal diameter rather than the external vessel diameter.

The recorded parameters were right and left P1 length, right and left P1 calibre, symmetry or dominance of P1 calibre, P1 hypoplasia, P1 agenesis, P1 fenestration, fetal-type PCA configuration, origin of the SCA from P1, and distribution pattern of posteromedial perforating branches. For the posteromedial perforators we propose a descriptive scheme developed for the present study, organised around two complementary criteria: (i) the internal organisation of the perforator group (multiple small branches vs few large trunks; symmetric vs asymmetric arrangement) and (ii) the crossing of the anatomical midline by one or more dominant trunks. This scheme is intended as an anatomical description that may facilitate future radiological–clinical correlation, but has not been validated against confirmed thalamic infarcts and should be regarded as exploratory. The framework refines, but does not replicate, earlier descriptive schemes by Saeki and Rhoton and by Marinković et al., which classified perforators by number and calibre but did not formally incorporate midline-crossing as a discriminating criterion (2,6). The five resulting types (I–V) are detailed in *Table 5* and discussed in the section *Perforator variability and thalamo-mesencephalic ischaemia*.

P1 hypoplasia and fetal-type PCA were treated as partially overlapping anatomical variables rather than mutually exclusive entities. P1 hypoplasia describes the calibre of the precommunicating segment, whereas fetal-type PCA describes the functional and haemodynamic relationship between P1 and the PComA. A partial fetal-type PCA usually includes a hypoplastic P1 segment associated with a dominant PComA, whereas a complete fetal-type PCA implies functional or anatomical absence of P1.

**Table 5.** Descriptive scheme of posteromedial perforating branches proposed in this study, based on internal organisation and crossing of the anatomical midline. This scheme is exploratory and has not been validated against clinical outcomes.

| Type | Anatomical description | Cases | % (n=320) |
|---|---|---|---|
| I | Multiple small branches (6–15) bilaterally, symmetric organisation, no midline-crossing trunk. | 74 | 23.1 % |
| II | Few large trunks (≤ 5), symmetric organisation, no midline-crossing trunk. | 51 | 15.9 % |
| III | Few large trunks, asymmetric, with one or more crossing the midline. | 94 | 29.4 % |
| IV | Asymmetric mixed pattern combining one or more dominant trunks with smaller satellite branches. | 96 | 30.0 % |
| V | Single common trunk arising from one P1 and supplying bilateral paramedian thalamic and rostral midbrain territories (artery of Percheron). | 5 | 1.6 % |
| Total | — | 320 | 100.0 % |

**Note.** Denominator N = 320 because posteromedial perforator pattern was assessed qualitatively across all three modalities. The proposed scheme is exploratory and requires future clinical–radiological validation.

A diameter below 1 mm was used as the operational threshold for P1 hypoplasia. This cut-off is in line with thresholds applied in previous angiographic and anatomical studies of hypoplastic segments of the circle of Willis (5,15,16,17). Some authors define fetal-type PCA on the relative P1/PComA diameter relationship rather than on an absolute P1 cut-off; the implications of this difference are discussed below (15,17).

The analysis of posteromedial perforating branches was based primarily on dissection findings and on high-quality angiographic reconstructions in which the perforator pattern was sufficiently visible. Small perforators that could not be reliably identified on CTA or MRA were not overinterpreted. The intrinsic limitation of in-vivo angiography for visualizing submillimetre perforators is addressed in the Discussion.

### *Symmetry Threshold*

Symmetry of P1 calibre was defined operationally as a right–left absolute difference of no more than 0.3 mm. This threshold was selected as approximately twice the smallest unit of measurement reproducible on the angiographic workstation in our pilot calibration and is consistent with criteria used in prior 3D TOF MRA series of the circle of Willis (5).

### *Measurement Reliability*

All morphometric measurements were performed by one investigator and independently reviewed by a second senior radiologist; cases in which the two readings disagreed were re-examined and resolved by consensus before the value was retained for analysis. The 0.3 mm threshold used to define right–left symmetry of P1 calibre and the 1 mm threshold used to define P1 hypoplasia were chosen on the basis of the smallest measurement increment that could be reproduced consistently on the angiographic workstation in our pilot calibration. Formal quantitative reproducibility analysis (interobserver and intraobserver intraclass correlation coefficients for continuous variables and Cohen's kappa for categorical variables) was not performed in the present study; this is acknowledged as a limitation.

### *Morphometric Inclusion Criteria*

Morphometric analysis included only cases in which the P1 segment could be identified and measured reproducibly. Differences between the denominators of the morphometric series were mainly explained by anatomical dissection cases in which vessel preparation, extraction, preservation, or incomplete vascular integrity prevented reliable measurement of P1 length or calibre, and by angiographic cases with motion or coverage artifacts. These cases were retained for qualitative anatomical description but excluded from quantitative morphometric calculations when measurement reliability was insufficient (see *Fig. 1*).

### *Statistical Analysis*

The primary analysis was descriptive. For continuous variables (P1 length and calibre), the number of available values, minimum, maximum, mean, sample standard deviation, median, and interquartile range (IQR) were reported separately for the right and left sides. Because individual case identifiers linking right- and left-sided measurements within the same case had not been retained at the morphometric-data-export stage, paired analysis at the individual level was not possible. Right- versus left-sided comparison of the morphometric distributions was therefore performed with the Mann–Whitney U test on independent samples, with the Welch t-test reported as a sensitivity analysis. This choice is acknowledged as a methodological limitation: the results support comparison of the overall right and left distributions but do not constitute a formal test of intra-individual symmetry. The Shapiro–Wilk test was used to assess the assumption of normality, which confirmed non-normal distributions for all morphometric variables ($p < 0.001$), supporting the use of a non-parametric test as the primary analysis. Categorical variables (hypoplasia, fetal-type, perforator pattern, SCA origin) were summarized as counts and percentages with 95 % Wilson confidence intervals. A two-sided p-value $< 0.05$ was considered statistically significant. Analyses were performed in Python 3.12 with SciPy 1.x (SciPy Developers).

### *Ethics Statement*

This study consisted of a retrospective analysis of previously acquired, fully anonymised anatomical and imaging material. The cadaveric specimens had been obtained through the institutional anatomy programme in accordance with national legal provisions and institutional regulations governing the donation, preservation and educational use of human anatomical material for research and teaching. The angiographic component consisted of the secondary analysis of fully anonymised CT and MR angiography datasets retrieved from the routine clinical archive of the institution; the datasets contained no direct or

indirect identifiers of the patients. Under the national regulatory framework and the institutional policy at Ovidius University of Constanța applicable at the time of the study, retrospective analyses of previously acquired anonymised material for descriptive anatomical purposes did not require prospective approval by the institutional Ethics Committee. All procedures conformed to the ethical standards of the 1964 Declaration of Helsinki and its later amendments. No individually identifiable patient data are presented in this manuscript.

## Results

### *Study Sample*

The study included 320 cases (*Table 1*). Anatomical dissections were performed on 20 formalin-fixed brain specimens, ten of which were plastic-injected to improve visualization of the arterial tree. The angiographic dataset consisted of 120 CT angiographies and 180 MR angiographies.

### *P1 Segment Length*

The numerical series for P1 length included 255 right-sided and 254 left-sided values. The mean length of the right P1 segment was 7.57 ± 2.24 mm (median 7.40 mm; IQR 6.20–8.65 mm). The mean length of the left P1 segment was 7.38 ± 2.19 mm (median 7.20 mm; IQR 6.00–8.60 mm). Extreme values were verified case-by-case and retained because they corresponded to true anatomical variants rather than to measurement or data-extraction artifacts.

On independent-samples comparison, no statistically significant difference was detected between the right and left P1 length distributions (Mann–Whitney U = 33 821, p = 0.387; Welch t-test p = 0.226). Shapiro-Wilk testing confirmed non-normality of both distributions ($p < 0.001$). Descriptive statistics are summarized in *Table 2*.

### *P1 Segment Calibre*

Two analyses were performed: one including hypoplastic segments and one excluding them. When hypoplastic segments were included, the right P1 series contained 259 values and the left P1 series contained 263 values. Mean calibre was 1.87 ± 0.59 mm on the right and 1.86 ± 0.57 mm on the left. After exclusion of hypoplastic segments, the mean calibre increased to 1.98 ± 0.48 mm on the right and 1.98 ± 0.43 mm on the left. The majority of P1 calibres (approximately 232/320 cases, 72.5 %) fell between 1.4 and 2.0 mm.

The independent-samples comparison did not detect a statistically significant right–left difference either when hypoplastic segments were included (Mann–Whitney U = 34 178, p = 0.945; Welch t-test p = 0.880) or when they were excluded (Mann–Whitney U = 28 432, p = 0.941; Welch t-test p = 0.858). These findings provide statistical support for the descriptive observation of broadly symmetric P1 calibre distributions between sides at the group level.

Descriptive statistics are summarized in *Table 3*.

### *Symmetry and Dominance of P1 Calibre*

Using a right–left absolute difference of no more than 0.3 mm as the criterion for symmetry, P1 calibre symmetry was observed in 212/320 cases (66.2 %; 95 % Wilson CI 60.9 – 71.2 %). Right-sided dominance was observed in 55/320 (17.2 %; 95 % CI 13.4 – 21.7 %) and left-sided dominance in 49/320 (15.3 %; 95 % CI 11.8 – 19.7 %; *Fig. 2*). Four cases (1.3 %; 95 % CI 0.5 – 3.2 %) remained borderline, with a right–left difference at the limit of measurement reproducibility. Descriptive statistics are summarized in *Table 4*.

### *P1 Hypoplasia, Fetal-type PCA, Agenesis, and Fenestration*

P1 hypoplasia (calibre < 1 mm) was identified in 51 cases (15.9 %; 95 % Wilson CI 12.3 – 20.4 %). Bilateral P1 hypoplasia was present in 10 cases (3.1 %; 95 % CI 1.7 – 5.7 %), right-sided unilateral hypoplasia in 22 cases (6.9 %; 95 % CI 4.6 – 10.2 %), and left-sided unilateral hypoplasia in 19 cases (5.9 %; 95 % CI 3.8 – 9.1 %). Representative angiographic appearances of the basilar bifurcation and bilateral P1 segments are illustrated in *Figs. 3* and *4*.

Fetal-type PCA was recorded as a separate haemodynamic-relationship variable. A bilateral fetal-type configuration was identified in 13 cases (4.1 %; 95 % Wilson CI 2.4 – 6.8 %) and a unilateral fetal-type configuration in 48 cases (15.0 %; 95 % CI 11.5 – 19.3 %; *Fig. 6*). P1 agenesis was observed in 6 cases (1.9 %; 95 % CI 0.9 – 4.0 %) and P1 fenestration in 3 cases (0.9 %; 95 % CI 0.3 – 2.7 %; *Fig. 7*). A representative variant configuration of the basilar apex with combined P1 abnormalities is shown in *Fig. 5*.

### *Posteromedial Perforating Branches*

Posteromedial perforating branches showed substantial variability. Five patterns were identified using the exploratory descriptive scheme proposed in this study (*Table 5*). Type IV (asymmetric mixed) was the most frequent pattern (*Fig. 8*), followed by type III

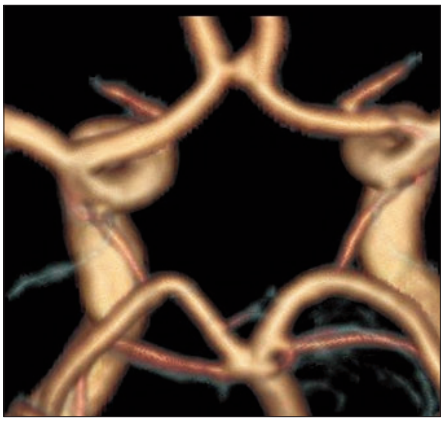

**Figure 2.** 3D MR angiography reconstruction: P1 segment calibre asymmetry with left side dominance

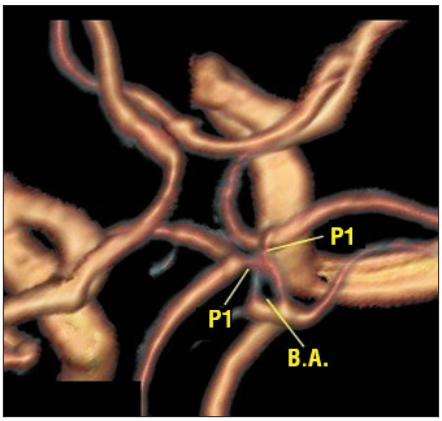


**Figure 3.** 3D MR angiography reconstruction: bilateral fetal type with bilateral P1 segment hypoplasia and basilar artery fenestration
P1 — precommunicating segment of the PCA, B.A. — basilar artery

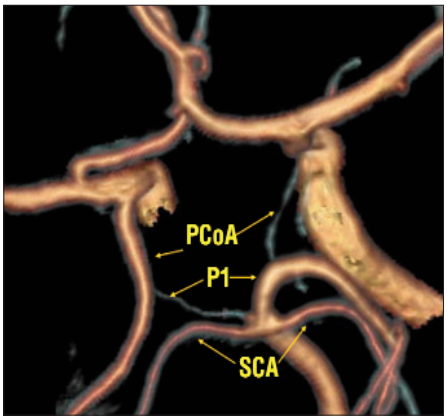


**Figure 4.** 3D CT angiography reconstruction: right P1 segment hypoplasia. P1 — precommunicating segment of the PCA, PCoA — posterior communicating artery, SCA — superior cerebellar artery

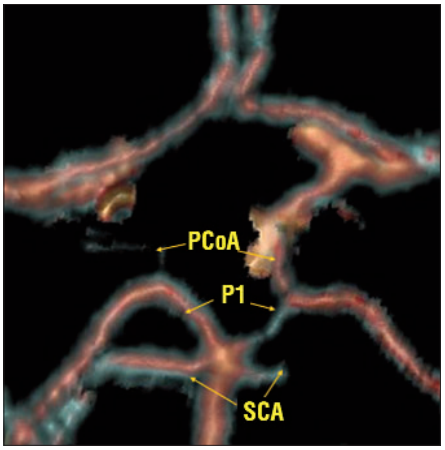


**Figure 5.** 3D CT angiography reconstruction: left P1 segment hypoplasia. P1 - precommunicating segment of the PCA, PCoA - posterior communicating artery, SCA - superior cerebellar artery

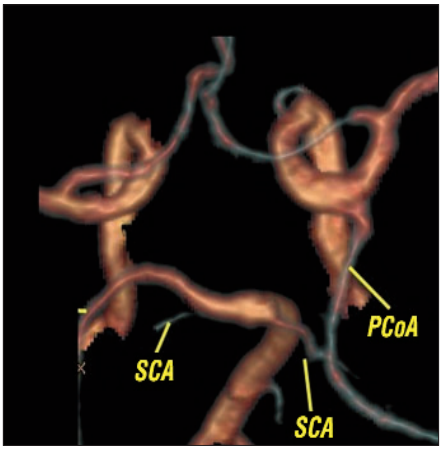


**Figure 6.** 3D MR angiography reconstruction: left P1 segment agenesis with unilateral fetal type, PCoA - posterior communicating artery, SCA - superior cerebellar artery

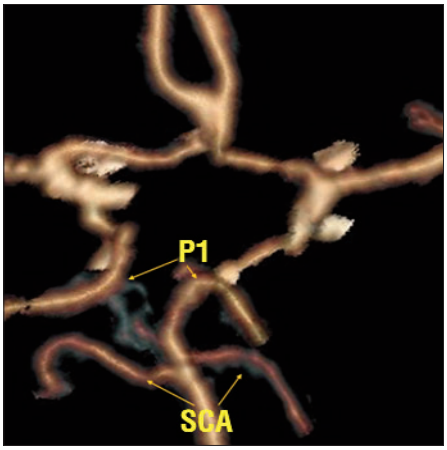


**Figure 7.** 3D CT angiography reconstruction: right P1 segment fenestration. P1 - precommunicating segment of the PCA, SCA - superior cerebellar artery

(asymmetric, midline-crossing; *Fig. 9*). Together, the asymmetric midline-crossing types III and IV represented 190 cases (59.4 %; 95 % Wilson CI 53.9 – 64.6 %). The artery of Percheron pattern (type V) was identified in 5 cases (1.6 %; 95 % CI 0.7 – 3.6 %; *Fig. 10*). These proportions describe the anatomical distribution observed in the present series; correlation with clinical stroke syndromes was not part of the study.

### *Origin of the Superior Cerebellar Artery from P1*

The SCA arose from the P1 segment in 25 cases (7.8 %; 95 % Wilson CI 5.4 – 11.3 %). Each hemisphere was systematically examined for both ipsilateral and contralateral SCA-from-P1 variants. The right SCA arose from the right P1 in 13 cases (4.1 %; 95 % CI 2.4 – 6.8 %; *Fig. 11*), the left SCA from the left P1 in 9 cases (2.8 %; 95 % CI 1.5 – 5.3 %), and the right SCA from the left P1 in 3 cases (0.9 %; 95 % CI 0.3 – 2.7 %; cross-midline variant; *Fig. 12*); no instance of the left SCA arising from the right P1 was identified in the present series.

This variation is relevant to basilar-apex surgery, angiographic interpretation, and endovascular navigation because it alters the expected relationship between the basilar bifurcation, P1, the SCA, and thalamo-mesencephalic perforators (1,2,18). Descriptive statistics are summarized in *Table 6*.

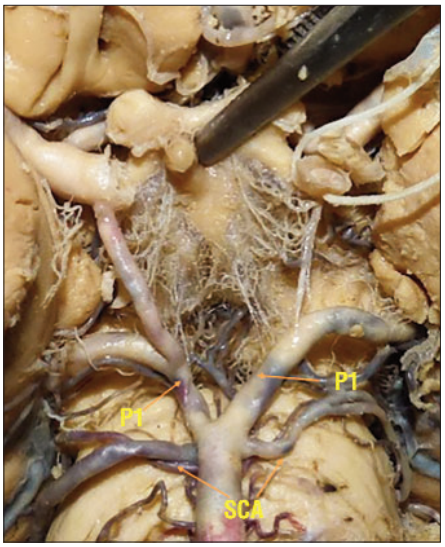


**Figure 8.** Brain dissection showing type IV distribution of deep perforating branches. P1 - precommunicating segment of the PCA, SCA - superior cerebellar artery

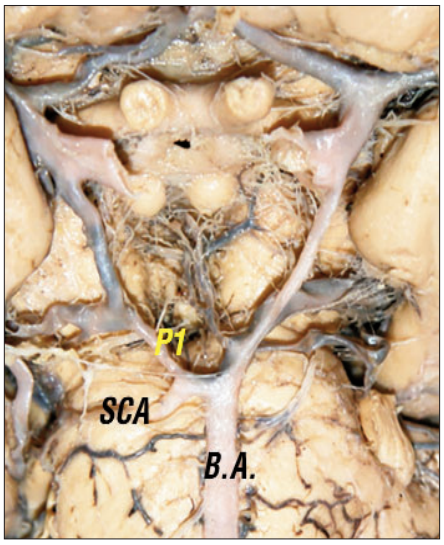


**Figure 9.** Brain dissection showing type III distribution of deep perforating branches. P1 - precommunicating segment of the PCA, SCA - superior cerebellar artery, .BA - basilar artery

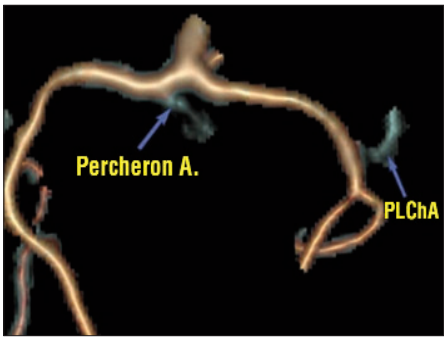


**Figure 10.** 3D MR angiography reconstruction: artery of Percheron arising from the right P1 segment PLChA – posterolateral choroidal artery.

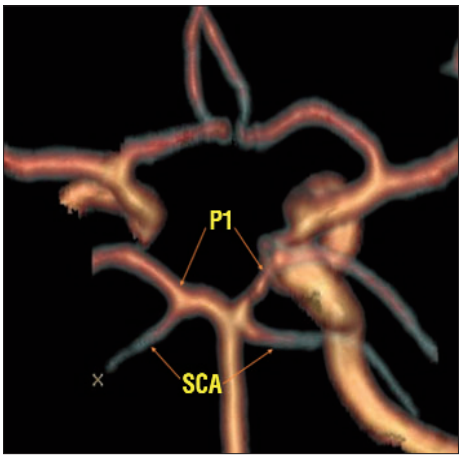


**Figure 11.** 3D MR angiography reconstruction: right superior cerebellar artery originating from the right P1 segment. P1 - precommunicating segment of the PCA, SCA - superior cerebellar artery

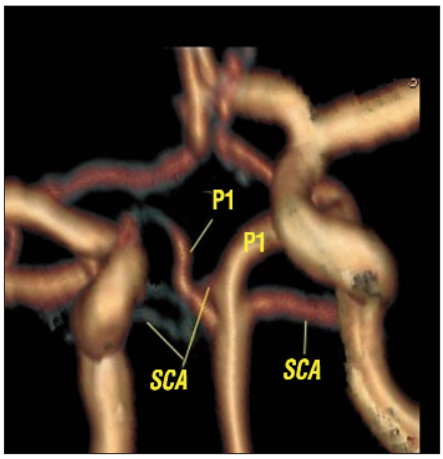


**Figure 12.** 3D MR angiography reconstruction: right superior cerebellar artery originating from the left P1 segment. P1 - precommunicating segment of the PCA, SCA - superior cerebellar artery

**Table 6.** Origin of the superior cerebellar artery from P1.

| Variant | Number of cases | Percentage (n=320) |
|---|---|---|
| Right SCA from right P1 (ipsilateral) | 13 | 4.1 % |
| Left SCA from left P1 (ipsilateral) | 9 | 2.8 % |
| Right SCA from left P1 (contralateral) | 3 | 0.9 % |
| Left SCA from right P1 (contralateral) | 0 | 0.0 % |
| Total SCA origin from P1 | 25 | 7.8 % |

## Discussion

### *Framework for the Clinical Correlation of P1 Anatomical Variants*

In the present study, clinical correlation is understood as the structured linkage between morphological variants documented in the anatomical and angiographic series and their known implications for radiological interpretation, stroke topography, aneurysm haemodynamics, and neurovascular procedures. This

usage follows the established tradition of surgical anatomy studies published in the anatomical and radiological literature, in which the term denotes a systematic mapping of anatomical structure onto clinical management, rather than direct outcome analysis of individual patients. The clinical correlations discussed in the following subsections are drawn from the published literature and applied to the variant frequencies observed in the present series; they are not derived from prospective clinical follow-up of the individuals whose imaging datasets were analysed. This distinction is made explicit here to allow the reader to interpret the clinical implications appropriately. Accordingly, any reference in this manuscript to the clinical relevance or clinical utility of the P1 anatomical variants - for radiological reporting, stroke topography, aneurysm haemodynamics, or neurovascular procedures — is anatomically motivated and hypothesis-generating. It does not represent clinical validation and should not be interpreted as such.

### *Morphometric Profile of the P1 Segment*

The present series demonstrates that the P1 segment has a relatively symmetric mean morphometric profile, with comparable right and left values for both length and calibre. The mean P1 length was 7.57 mm on the right and 7.38 mm on the left. Mean P1 calibre, including hypoplastic segments, was 1.87 mm on the right and 1.86 mm on the left, rising to 1.98 mm bilaterally after exclusion of hypoplastic segments.

These findings support the predominance of an adult-type posterior circulation pattern in most cases. However, the wide range of values and the presence of anatomical extremes indicate that average values alone are insufficient for clinically relevant interpretation. In practice, a very small P1 segment may indicate hypoplasia or fetal-type PCA, whereas a large P1 may reflect a dominant basilar contribution to the PCA territory.

The morphometric values obtained in the present series are broadly comparable with previously published anatomical and angiographic studies, although direct comparison is constrained by methodological differences in measurement technique and case selection (*Table 7*). The slightly higher upper limits in our series reflect the inclusion of true anatomical extremes retained in the angiographic dataset. Mean P1 length is somewhat greater in our angiographic dataset than in the recent cadaveric series of Nas et al., which is compatible with the known systematic difference between in-vivo angiographic measurement (along the curved central axis with full luminal opacification) and ex-vivo dissection measurement (after fixation-induced shortening) (12,13).

### *Hypoplasia, Fetal-type PCA, Agenesis and Fenestration*

The distinction between P1 hypoplasia and fetal-type PCA is conceptual and practical. P1 hypoplasia describes the calibre of the precommunicating segment; fetal-type PCA describes the functional dominance of the PComA over P1. The two features frequently overlap but are not identical (*Table 8*). This distinction is important for radiologists, neurologists, and neurosurgeons because a fetal-type PCA modifies embolic pathways, ischaemic territories, and procedural risk.

**Table 7.** Consolidated comparison with previously published anatomical, angiographic and variant-configuration data.

| Study | Method | Sample | Length data | Calibre data | Fetal-type / variants | Ref. |
|---|---|---|---|---|---|---|
| Present study | Dissection + CTA + MRA | 320 | R 7.57 ± 2.24 mm; L 7.38 ± 2.19 mm | R 1.87 ± 0.59 mm; L 1.86 ± 0.57 mm (incl. hypoplasia) | Unilateral fetal-type 15.0 %; bilateral 4.1 %; P1 agenesis 1.9 % | — |
| Krishnamurthy et al. 2008 | Cadaveric dissection | 89 | Mean PCA 6.75 ± 1.48 mm | Mean PCA 1.7 ± 0.7 mm | — | (10) |
| Dodevski et al. 2014 | CT angiography | 53 | Not primarily reported | R 1.74 ± 0.32 mm; L 1.98 ± 0.41 mm | Fetal-type 22.64 % | (11) |
| Gunnal 2015 | Cadaveric dissection | 340 PCAs | Mean P1 length reported per side | Hypoplasia 5.29 %; aplasia 2.35 % | Fetal-type described qualitatively | (15) |
| Coulier 2021 | CTA, large retrospective | 2125 | Configuration analysis | Imaging-based P1/PComA ratios | Fetal-type PCA analysis based on ratios | (16) |
| Nas et al. 2024 (SRA) | Cadaveric morphometry, ImageJ | 170 cadavers / 340 hemispheres | R 5.97 ± 2.18 mm; L 6.24 ± 2.64 mm | P1/PComA configuration-based classification | Configuration-based reporting | (12) |
| Nas et al. 2024 (World Neurosurg) | Fresh-cadaver morphometry | 170 cadavers | PCA and basilar morphometry | PCA and basilar diameter, fresh-tissue | — | (13) |

**Abbreviations:** CTA, computed tomography angiography; MRA, magnetic resonance angiography; PCA, posterior cerebral artery; PComA, posterior communicating artery; R, right; L, left

**Table 8.** P1 hypoplasia, fetal-type PCA, agenesis and fenestration: anatomical criteria, haemodynamic interpretation, and observed frequencies in the present series. Categories overlap conceptually; percentages should not be summed as independent events.

| Variant / Configuration | Anatomical criterion | Haemodynamic interpretation | Cases | % (n = 320) |
|---|---|---|---|---|
| P1 hypoplasia (any) | P1 calibre < 1 mm | Reduced basilar contribution to the PCA territory; may coexist with partial fetal-type PCA | 51 | 15.9 % |
| Bilateral P1 hypoplasia | Bilateral P1 calibre < 1 mm | Bilaterally reduced basilar contribution to both PCA territories | 10 | 3.1 % |
| Right P1 hypoplasia | Right P1 calibre < 1 mm | Right-sided reduced basilar contribution | 22 | 6.9 % |
| Left P1 hypoplasia | Left P1 calibre < 1 mm | Left-sided reduced basilar contribution | 19 | 5.9 % |
| P1 agenesis | No identifiable precommunicating P1 segment | Complete carotid supply of the ipsilateral distal PCA when PComA is dominant (complete fetal-type) | 6 | 1.9 % |
| P1 fenestration | Segmental duplication of the arterial lumen | Local variant of arterial morphology; may modify local haemodynamics | 3 | 0.9 % |
| Bilateral fetal-type PCA | Bilateral PComA dominance over P1 | Bilateral carotid supply of the distal PCA territories | 13 | 4.1 % |
| Unilateral fetal-type PCA | Unilateral PComA dominance over P1 | Unilateral carotid supply of the distal PCA territory | 48 | 15.0 % |

The observed frequencies of P1 hypoplasia (15.9 %), unilateral fetal-type PCA (15.0 %), and bilateral fetal-type PCA (4.1 %) are in the range reported by previous large angiographic and anatomical series, although exact percentages vary with the definition used and the imaging technique (10,11,15-17). The variability of published estimates further supports the need for a consistent operational definition, which was one aim of the present descriptive study.

P1 agenesis, observed in 1.9 % of cases, represents the anatomical substrate of a complete fetal-type PCA configuration when the PComA is dominant. P1 fenestration, identified in 0.9 % of cases, is a rare variant that may be under-detected on standard imaging and has been associated with an increased risk of aneurysmal degeneration at the fenestration site (18,19).

### *Perforator Variability and Thalamo-Mesencephalic Ischemia*

Posteromedial perforators arising from the P1 segment supply the paramedian thalamus and rostral midbrain. Their variability has direct implications for the topography of thalamo-mesencephalic infarcts and for the surgical approach to the basilar apex (2,6,7,14). The descriptive scheme proposed in this study organises the observed patterns around two anatomical criteria — internal organisation and midline crossing — and yields five types with frequencies of 23.1 %, 15.9 %, 29.4 %, 30.0 %, and 1.6 %, respectively (*Table 5*).

The artery of Percheron pattern (5 cases, 1.6 %) is a well-known cause of bilateral paramedian thalamic infarction with characteristic clinical presentation including altered consciousness, memory disturbance, and vertical gaze impairment (14). Its identification on cross-sectional imaging is challenging because of the small calibre of the trunk; awareness of the variant improves prospective radiological detection.

### *Origin of the SCA from P1*

An SCA origin from P1 was identified in 7.8 % of cases, including three contralateral (cross-midline) variants. This proportion is comparable to previous cadaveric and angiographic series (1,2,18). From a clinical standpoint, this variant is relevant for the interpretation of basilar-apex aneurysms, endovascular navigation, and microsurgical planning, because the expected relationship between the basilar bifurcation, P1, SCA, and posteromedial perforators is altered.

### *Study Limitations*

The findings of this study should be interpreted in the light of the following limitations, which are declared explicitly:

1. Right-left morphometric comparisons were performed on independent samples (Mann-Whitney U test) because individual case-level identifiers linking right- and left-sided measurements within the same individual had not been retained at the morphometric-data-export stage. Tests on independent samples cannot demonstrate intra-individual symmetry; the reported results support comparison of the overall right and left distributions only, and should not be interpreted as evidence of paired symmetry within cases.
2. Patient-level population characteristics were not linked to the anatomical measurements. Age, sex, clinical indication for the imaging examination, associated vascular pathology, temporal criteria of selection and sampling

scheme are therefore not reported, which limits the assessment of selection bias and the generalisability of the findings.

3. A formal reproducibility analysis was not performed. Interobserver and intraobserver intraclass correlation coefficients for continuous variables, and Cohen's kappa for categorical classifications, were not computed on a remeasured subsample; reproducibility was addressed only by independent dual review with consensus adjudication.
4. The 0.3 mm and 1 mm operational thresholds used to define right–left symmetry of P1 calibre and P1 hypoplasia, respectively, are close to the resolution limit of the imaging technique and have not been formally validated by an experimental measurement-reliability study; they should be regarded as pragmatic thresholds pending future validation.
5. The three modalities (cadaveric dissection, CTA, MRA) were not analysed as stratified subgroups with separate numerical outputs. The angiographic dataset (CTA + MRA) was analysed jointly, and the cadaveric subset contributed only qualitative variant identification. Full per-modality stratification with modality-specific frequencies is not reported and is identified as a target for a future analysis.
6. The five-type descriptive scheme of posteromedial perforating branches proposed in this study is exclusively exploratory. It has not been validated by external clinical radiological correlation with confirmed thalamic infarcts, and its reproducibility has not been assessed by an independent observer group; it should be regarded as a morphological framework for future validation rather than as a validated classification.
7. The observed frequency of SCA origin from P1 (7.8 %) is at the upper end of the range reported in the literature and would benefit from confirmation in an independent cohort with strict anatomical definition, high-quality representative images and per-modality analysis, to exclude conflation with a common P1–SCA trunk, with an origin very close to the basilar bifurcation, or with a reconstruction artefact.
8. The denominators of the morphometric variables differ from the total sample size (n = 320) because only the angiographic subset (CTA + MRA, n = 300) contributed morphometric measurements, and a small number of angiographic cases were further excluded because of measurement reliability. Actual evaluable denominators are shown explicitly in every morphometric table, in the STROBE-style flow diagram (*Fig. 1*), and in the corresponding table notes.
9. The present study did not analyse the influence of age, sex or associated pathology on the observed anatomical variants; the anonymised nature of the dataset precluded this analysis. Such determinants should be explored in a future prospective sub-study with case-level identifiers and demographic linkage.
10. This is a single-centre study performed with a single 128-slice CT scanner and a single 1.5 T MR system. Multicentre validation across different scanner platforms and field strengths would further support the generalisability of the morphometric thresholds and of the proposed perforator scheme.
11. The clinical correlation component of this study is a structured narrative synthesis based on the published literature applied to the variant frequencies observed in the present series. It does not include prospective clinical follow-up of the individuals whose imaging datasets were analysed, and it does not constitute original clinical outcome data.
12. Any statement in this manuscript regarding the clinical utility of P1 anatomical variants - for radiological reporting, stroke topography, aneurysm haemodynamics, or neurovascular procedures — should be understood as anatomically motivated and hypothesis-generating. It does not constitute evidence of clinical validation, and should not be interpreted as such by the reader.

## Conclusions

The P1 segment of the posterior cerebral artery exhibits a broadly symmetric mean morphometric profile but harbours a wide spectrum of clinically relevant variants. Hypoplasia (15.9 %), fetal-type PCA (unilateral 15.0 %, bilateral 4.1 %), agenesis (1.9 %), fenestration (0.9 %), asymmetric perforator patterns (59.4 %), the artery of Percheron (1.6 %), and SCA origin from P1 (7.8 %) were sufficiently frequent to warrant systematic reporting of the P1-PComA complex on cross-sectional angiography. The descriptive perforator scheme proposed in this study offers a framework for future clinical–radiological validation and should not be interpreted as a validated classification until such validation is completed. Awareness of these variants is relevant for radiological interpretation, stroke topography, aneurysm haemodynamics, and the planning of basilar-apex procedures.

### *Author's Contributions*

All authors contributed equally to this work. Each author was involved in the conception and design of the study, the acquisition, analysis and interpretation of the anatomical and angiographic data and the drafting and critical revision of the manuscript for important intellectual content. All authors approved the final version of the manuscript and agree to be accountable for all aspects of the work in accordance with the International Committee of Medical Journal Editors (ICMJE) recommendations on authorship.

### *Acknowledgments*

The authors thank the staff of the Department of Anatomy, Faculty of Medicine, Ovidius University of Constanța, for their assistance with specimen preparation.

### *Conflicts of Interest*

The authors declare that they have no competing interests, financial or non-financial, that are relevant to the content of this article.

### *Funding*

The authors did not receive any specific grant or financial support from public, commercial, or not-for-profit funding agencies for this study.

### *Consent to participate / Consent for publication*

Not applicable. This study involved the retrospective analysis of previously acquired, fully anonymised anatomical and imaging material, and no individually identifiable patient data are presented. Under the applicable national regulatory framework and institutional policy, prospective approval by the institutional Ethics Committee was not required for retrospective descriptive analyses of previously acquired anonymised material. The cadaveric specimens were used in accordance with national and institutional regulations governing the use of human anatomical material for research and teaching.

### *Data Availability*

The anonymised anatomical and morphometric datasets analysed during the current study are available from the corresponding author on reasonable request, subject to institutional data-sharing regulations.

## References

1. Rhoton AL Jr. The supratentorial arteries. Neurosurgery. 2002;51(4 Suppl):S53–S120.
2. Marinković S, Milisavljević M, Marinković Z. Anatomical bases for surgical approach to the initial segment of the posterior cerebral artery. Microarterial anatomy and clinical relevance. Surg Radiol Anat. 1990;12(2):125–133.
3. Zeal AA, Rhoton AL Jr. Microsurgical anatomy of the posterior cerebral artery. J Neurosurg. 1978;48(4):534–559.
4. Alpers BJ, Berry RG, Paddison RM. Anatomical studies of the circle of Willis in normal brain. AMA Arch Neurol Psychiatry. 1959;81(4):409–418.
5. Krabbe-Hartkamp MJ, van der Grond J, de Leeuw FE, de Groot JC, Algra A, Hillen B, et al. Circle of Willis: morphologic variation on three-dimensional time-of-flight MR angiograms. Radiology. 1998;207(1):103–111.
6. Saeki N, Rhoton AL Jr. Microsurgical anatomy of the upper basilar artery and the posterior circle of Willis. J Neurosurg. 1977;46(5):563–578.
7. Pedroza A, Dujovny M, Ausman JI, Diaz FG, Cabezudo Artero J, Berman SK, et al. Microvascular anatomy of the interpeduncular fossa. J Neurosurg. 1986;64(3): 484–493.
8. van Overbeeke JJ, Hillen B, Tulleken CAF. A comparative study of the circle of Willis in fetal and adult life. The configuration of the posterior bifurcation of the posterior communicating artery. J Anat. 1991;176:45–54.
9. Kapoor K, Singh B, Dewan LIJ. Variations in the configuration of the circle of Willis. Anat Sci Int. 2008;83(2):96–106.
10. Krishnamurthy A, Nayak SR, Bhat S, Somayaji SN, Prabhu LV, Rai R, et al. Morphological variations of the posterior cerebral artery: an anatomical study. Neuroanatomy. 2008;7:22–25.
11. Dodevski A, Lazareska M, Tosovska-Lazarova D, Zhivadinovik J, Stojkoski A. Morphological characteristics of the posterior cerebral artery. Prilozi. 2014;35(2): 119–124.
12. Nas OF, Kilincer A, Ozdemir M. Morphometric analysis of the posterior cerebral artery and its P1 segment on cadaveric specimens. Surg Radiol Anat. 2024;46(2):203–212.
13. Nas OF, Kilincer A, Ozdemir M, Erdem G. Fresh-cadaver morphometric analysis of the posterior cerebral and basilar arteries. World Neurosurg. 2024;181:e412–e421.
14. Percheron G. Les artères du thalamus humain. II. Artères et territoires thalamiques paramédians de l'artère basilaire communicante. Rev Neurol (Paris). 1976;132(5): 309–324.
15. Gunnal SA, Farooqui MS, Wabale RN. Anatomical variations of the circulus arteriosus in cadaveric human brains. Neurol Res Int. 2015;2015:687492.
16. Coulier B. Fetal-type variants of the posterior cerebral artery on CT angiography: analysis of a large retrospective series. J Belg Soc Radiol. 2021;105(1):55.
17. Lazzaro MA, Ouyang B, Chen M. The role of circle of Willis anomalies in cerebral aneurysm rupture. J Neurointerv Surg. 2012;4(1):22–26.
18. Caruso G, Vincentelli F, Rabehanta P, Giudicelli G, Grisoli F. Anomalies of the P1 segment of the posterior cerebral artery: early bifurcation or duplication, fenestration, common trunk with the superior cerebellar artery. Acta Neurochir (Wien). 1991; 109(1–2):66–71.
19. Kai Y, Hamada J, Morioka M, Yano S, Kudo M, Kuratsu J. Basilar artery apex fenestration: a rare cause of aneurysm. Neuroradiology. 2003;45(4):254–256.
20. van der Zwan A, Hillen B, Tulleken CA, Dujovny M, Dragovic L. Variability of the territories of the major cerebral arteries. J Neurosurg. 1992;77(6):927–940.
21. Yaşargil MG. Microneurosurgery: Volume I. Microsurgical Anatomy of the Basal Cisterns and Vessels of the Brain, Diagnostic Studies, General Operative Techniques and Pathological Considerations of the Intracranial Aneurysms. Stuttgart: Thieme; 1984.
22. Osborn AG. Diagnostic Cerebral Angiography. 2nd ed. Philadelphia: Lippincott Williams & Wilkins; 1999.
23. Bogousslavsky J, Regli F, Uske A. Thalamic infarcts: clinical syndromes, etiology, and prognosis. Neurology. 1988;38(6):837–848.
24. Schmahmann JD. Vascular syndromes of the thalamus. Stroke. 2003;34(9): 2264–2278.